Drastic Enhancement of Magnetic Critical Temperature and Amorphization in Topological Magnet $EuSn_2P_2$ under Pressure

Wenli Bi[1,*], Trenton Culverhouse[1], Zachary Nix[1], Weiwei Xie[2], Hung-Ju Tien[3], Tay-Rong Chang[3,4,5], Utpal Dutta[1], Jiyong Zhao[6], Barbara Lavina[6,7], Esen E. Alp[6], Dongzhou Zhang[8], Jingui Xu[8], Yuming Xiao[9], and Yogesh K. Vohra[1]

[1]Department of Physics, University of Alabama at Birmingham, Birmingham, AL 35294, USA
[2]Department of Chemistry and Chemical Biology, The State University of New Jersey-Rutgers, Piscataway, NJ 08854 USA
[3]Department of Physics, National Cheng Kung University, Tainan 701, Taiwan
[4]Center for Quantum Frontiers of Research and Technology, Tainan 701, Taiwan
[5]Physics Division, National Center for Theoretical Sciences, National Taiwan University, Taipei 10617, Taiwan
[6]Advanced Photon Source, Argonne National Laboratory, Argonne, IL 60439, USA
[7]Center for Advanced Radiation Sources, The University of Chicago, Chicago, IL 60637, USA
[8]Hawaii Institute of Geophysics and Planetology, School of Ocean and Earth Science and Technology, University of Hawaii at Manoa, Honolulu, Hawaii 96822, USA
[9]HPCAT, X-ray Science Division, Argonne National Laboratory, Argonne, Illinois 60439, USA

[*]wbi@anl.gov

ABSTRACT

High pressure is an effective tool to induce novel and exotic quantum phenomena in magnetic topological insulators by controlling the interplay of magnetic order and topological state. This work presents a comprehensive high-pressure study of the crystal structure and magnetic ground state up to 62 GPa in an intrinsic topological magnet $EuSn_2P_2$. With a combination of high resolution X-ray diffraction, ^{151}Eu synchrotron Mössbauer spectroscopy, X-ray absorption spectroscopy, molecular orbital calculations, and electronic band structure calculations, it has been revealed that pressure drives $EuSn_2P_2$ from a rhombohedral crystal to an amorphous phase at 36 GPa accompanied by a four-fold enhancement of magnetic ordering temperature. In the pressure-induced amorphous phase, Eu ions take an intermediate valence state. The drastic enhancement of magnetic ordering temperature from 30 K at ambient pressure to 130 K at 41.2 GPa resulting from Ruderman-Kittel-Kasuya-Yosida (RKKY) interactions likely attributes to the stronger Eu-Sn interaction at high pressure. These rich results demonstrate that $EuSn_2P_2$ is an ideal platform to study the correlation of the enhanced RKKY interactions, disordered lattice, intermediate valence, and topological state.

INTRODUCTION

Topological materials have recently emerged as a new frontier of condensed matter physics and materials research due to their rich quantum phases and potential applications in future dissipationless topological electronics and quantum computations (for reviews see ref.[1,2]). Among them, intrinsic magnetic topological systems are particularly interesting due to the potential applications in spintronic devices. Compared to dilute magnetic topological insulators, intrinsic magnetic materials are stoichiometric magnetic compounds that provide an easily synthesized, tunable, and clean platform to study magnetic topological materials with new intriguing quantum states. Such intrinsic magnetic topological materials are generally narrow-gap

semiconductors that combine nontrivial band topology and intrinsic magnetic order[3]. The intriguing interplay between magnetic ordering and topological states can generate exotic topological quantum phenomena, such as the quantum Hall effect[4–6], axion electrodynamics[7–10], and Majorana states[11]. Efforts in the study of emergent phenomena in intrinsic magnetic topological systems are mostly focused on $MnBi_2Te_4$[6,9,12–14] due to the very few available candidate materials. Very recently, a series of Eu-based compounds have been demonstrated experimentally, or proposed theoretically, to be intrinsic topological semimetals[5,15–18]. Among them, $EuSn_2P_2$ has been shown to be a magnetic topological system with type-A antiferromagnetic (AFM) order below 30 K[15]. $EuSn_2P_2$ crystallizes in a layered rhombohedral structure with space group of $R\bar{3}m$, similar to the A_2B_3 family of topological insulators[19]. It is comprised of strongly magnetic Eu layers sandwiched between Sn-P layers. Traditionally, Eu-based intermetallic materials have achieved considerable interest for their rich properties including magnetic phases from the strong local moment, valence transition, superconductivity, heavy-fermion states, and Kondo physics[20]. Despite of the rich quantum phenomena, much work is needed to understand the intriguing properties. In this work pressure is employed to control the crystal structure, magnetic, and valence states. Pressure has been proven to be a clean and effective way to tune the atomic distances and therefore electronic interactions to induce novel quantum phenomena in materials, such as superconductivity, magnetism, or electronic topological transitions. For example, pressure-induced suppression of Néel temperature and the emergence of superconductivity have been observed in magnetic compounds including heavy fermions and iron-based superconductors[21,22].

Here we report the first systematic high-pressure investigation in $EuSn_2P_2$ using a combined experimental approach including angular-dispersive X-ray diffraction (XRD), time-domain synchrotron Mössbauer spectroscopy (SMS), partial fluorescence-yield X-ray absorption spectroscopy (PFY-XAS), and molecular orbital and electronic band structure calculations. In $EuSn_2P_2$, the rhombohedral crystal structure remains stable up to 33 GPa before transforming to an amorphous phase. Surprisingly, an impressive over four-fold enhancement in magnetic ordering temperature (T_o) from 30 K at ambient pressure to 130 K at 41.2 GPa has been observed, despite of an increased mean valence above 20 GPa. The enhancement of magnetic exchange interaction is likely attributed to the stronger Eu-Sn interaction under pressure. This comprehensive study presents intriguing interplay of crystal structure, magnetic ground state, and the associated valence state tuned by high pressure.

RESULTS

Pressure-induced crystalline to amorphous transition

The evolution of structural properties of $EuSn_2P_2$ under hydrostatic pressure has been investigated by high resolution XRD experiments. The XRD data reveal that the ambient rhombohedral structure is maintained under pressure up to 33 GPa. At higher pressure the sample loses the long range crystalline order and becomes amorphous at 36 GPa, evidenced by the loss of sharp crystalline diffraction peaks (see Fig.1). With further compression the amorphous phase persists up to 62 GPa, the highest pressure measured in this study. The observed pressure-induced amorphization (PIA) contrasts with the rhombohedral-to-monoclinic transition reported in $EuSn_2As_2$[23]. The lattice parameters, interatomic distances, and unit cell volume of $EuSn_2P_2$ in the crystalline phase obtained from the Rietveld refinements from both XRD runs are plotted as a function of pressure (Fig.2). Parameters from run 1 with helium as hydrostatic pressure medium and run 2 with neon as quasihydrostatic pressure medium agree reasonably well. Using the third-order Birch-Murnaghan equation[24] a fit to the volume versus pressure data gives bulk modulus B_0 = 58 (2) GPa, its pressure derivative B'_0 = 3.6 (1) and volume at zero pressure V_0 = 375.1 (9) Å^3.

PIA has been documented in a wide variety of systems such as ice[25], $AlPO_4$[26,27], SnI_4[28], VO_2[29] and $EuIn_2As_2$[30]. The PIA may be related to structural instability violating Born stability criteria[28] or related to density/entropy-driven liquid phase[25,31]. However, the operative mechanism remains an open question in many cases. Additional experimental and computational investigation of variables (charge, orbital, elastic stability) could potentially help to gain a comprehensive understanding of the driving mechanism of PIA in $EuSn_2P_2$.

Drastic enhancement of T_o

Typical SMS spectra at selected pressures across T_o are presented in Fig.3. The SMS spectra were analyzed using CONUSS[32] by modeling the data with two sets of hyperfine parameters, magnetic hyperfine field (H_{hf}) and quadrupole splitting along with sample thickness. In the presence of magnetic ordering, quantum oscillations emerge in the time domain SMS spectrum due to nuclear Zeeman splitting. The analysis shows that the direction of magnetic hyperfine field is perpendicular to the X-ray propagation direction and lies in the ab-plane at ambient pressure, consistent with the results from neutron diffraction experiments at ambient pressure[15]. And this direction remains up to 42.7 GPa, the highest pressure reached, indicating Eu spins remain in-plane. When $EuSn_2P_2$ is warmed above T_o, H_{hf} drops to zero. The periodic oscillations in the data at 16.4 GPa and 96 K indicate a minor oxide impurity phase present in the sample used in run 2, which shows absence of magnetic hyperfine field and can be modeled with two paramagnetic sites with different isomer shift values, one from the sample and another from the impurity phase. In the magnetic phase a small quadrupole splitting of 1-5 mm/s has been included to fit the spectra. The temperature dependence of the extracted magnetic hyperfine field at various pressures is shown in Fig.4. With increasing pressure, T_o increases monotonically. It is remarkable that a moderate pressure of 41.2 GPa drives T_o to 130 K from 30 K at ambient pressure, a more than four-fold enhancement.

Valence state of Eu ions

To provide information on the valence state of Eu ions based on the isomer shift of ^{151}Eu, additional SMS spectra were taken simultaneously from the sample in the diamond anvil cell located inside the cryostat and the Eu_2O_3 reference placed outside of the cryostat and downstream of sample. The isomer shift is proportional to the electron density (dominated by *s* electrons) at the nucleus. The large separation of isomer shift values for Eu^{2+} and Eu^{3+}, resulting from different shielding effect of the closed-shell *s*-electrons by the $4f^7$ and $4f^6$ configurations, makes it useful to probe the valence based on the isomer shift value. Fig.5 displays such SMS spectra at various pressures and temperatures as well as corresponding simulated energy-domain spectra showing the changes of the isomer shift values of the sample with increasing pressure and the fixed isomer shift of reference sample Eu_2O_3. A monotonic increase of isomer shift from -10.3 mm/s at 1.0 GPa, 300 K to -5.39 mm/s at 41.2 GPa, 160 K has been observed (see Table.1). Caution needs to be taken when interpreting the change of isomer shift as change in valence state by simply assuming the contribution solely originating from the change in 4*f* electrons. For example, in pure Eu metal significant change in isomer shift was observed without obvious change in 4*f* electron occupancy[33].

To probe the valence state directly, PFY-XAS experiments at Eu's L_3 edge ($2p_{3/2} \rightarrow 5d$ transition) were carried out up to 47 GPa. The normalized high-pressure PFY-XAS data are shown in Fig.6. Eu ions in $EuSn_2P_2$ remain mostly divalent up to 19.8 GPa, indicating that the change in isomer shift at lower pressure is largely due to compression effect without involving the 4*f* electrons. At 19.8 GPa a second absorption peak emerges at ~8 eV higher in energy and grows with increasing pressure, indicating a transition toward Eu^{3+}. The 8 eV shift corresponds

to the excitation energy difference for $Eu^{3+}(4f^{6}5d^{1})$ and for $Eu^{2+}(4f^{7}5d^{0})$. Due to the decrease of absorption peak intensity under pressure, it is difficult to estimate the mean valence based on the ratio of the peak intensities. However, combining the PFY-XAS and change in the isomer shift value, it is safe to conclude that Eu take an intermediate valence state above 20 GPa. An accurate evaluation of the valence would require detailed electronic calculations under pressure.

Pressure-enhanced RKKY interaction

The magnetic order in $EuSn_2P_2$ at ambient pressure is driven by indirect Ruderman-Kittel-Kasuya-Yosida (RKKY) exchange coupling through spin-polarized conduction band. To provide insight to the enhanced T_o, we have performed molecular orbital calculations to illustrate the chemical bonding evolution at high pressure. The generated molecular orbitals diagrams containing the degenerated highest occupied molecular orbitals (HOMOs) and the lowest unoccupied molecular orbitals (LUMOs) of $EuSn_2P_2$ at ambient pressure and 23.3 GPa are shown in Fig.7. The HOMOs and LUMOs diagrams reflect the orbital interactions just below and above Fermi level, respectively. The blue and red colors indicate the contrast of the orbital symmetry, i.e., antibonding interactions. At both ambient and high pressure, the antibonding characters from Eu-4*f* orbitals are dominant among intralayer Eu atoms in HOMOs. $EuSn_2P_2$ can be viewed as Eu^{2+} cation packed with $(SnP)_2^{2-}$ anion along *c*-axis primarily by ionic bonding interactions from a charge balance view. Specifically, in chemistry Eu and P atoms are bonded ionically, Sn and P atoms are bonded covalently, and Eu and Sn atoms are bonded metallically. Near Fermi level the bonding interaction features can be observed between Eu-Sn and Eu-P at ambient pressure. When pressurized, $EuSn_2P_2$ exhibits stronger metallic Eu-Sn bonding interaction and a weaker covalent Sn-Sn bonding feature. Moreover, the distance between Eu-P atoms decreases, likely due to the 3*p* electronic localization on P induced by pressure. It suggests that pressure-enhanced Eu-Sn bonding interaction contributes to the increasing RKKY interaction and therefore enhanced T_o. This is consistent with the monotonic decrease of distances of Eu-Sn and Eu-P shown in Fig. 2 (c). Due to the much shorter intralayer Eu-Eu distance than interlayer Eu-Eu distance which leads to stronger intralayer magnetic exchange interaction than interlayer interaction, it is expected that the enhanced intralayer exchange interaction play a more important role in the increase of T_o, as concluded in the case of $EuIn_2As_2$[30]. In addition, the pressure-induced weakening of the ionic and covalent bonding and enhancement of metallic properties in $EuSn_2P_2$ may drive the crystal structure into amorphous phase, similar to amorphous magnets where the magnetic order is maintained in the amorphous phase[34].

Band structure calculations

The surface states and spin texture of $EuSn_2P_2$ from Eu termination were calculated using the Generalized Gradient approximation (GGA) plus correlation parameter (U = 6 eV) with spin-orbit coupling (SOC). According to the calculation, as the pressure is increased, the decreasing atomic distance along ab-plane may influence the topological properties if the in-plane magnetic spin orientation is maintained under pressure (Fig. S1). On the other hand, slightly spin canting along c-axis from the Eu layers may change the topological properties completely, consistent with the recent experimental and computational study in $EuSn_2P_2$[35].

Pressure phase diagram

Fig.8 presents the phase diagram constructed by combining the XRD, SMS, and PFY-XAS studies under pressure. The boundary between paramagnetic and magnetic phases is deduced from Fig.4. T_o shows a monotonic increase with pressure application with more than four times of the value at ambient pressure. Above 20 GPa a clear slope change in dT_o/dP coincides with transition from Eu^{2+} toward Eu^{3+} in Eu's valence based on the PFY-XAS data. Strikingly,

magnetic order is found to persist in the amorphous phase at 42.7 GPa. In another topological magnetic material, $EuIn_2As_2$, pressure-induced hexagonal-to-amorphous transition has been observed above 17 GPa with absence of magnetic order in the amorphous phase based on electrical resistivity measurements[30]. The PIA observed in both systems may suggest a similar origin of crystal structure instability. Furthermore, in the crystalline phase of $EuIn_2As_2$ a large enhancement of T_o is attributed to the increase of intraplane exchange interaction, consistent with the enhanced Eu-Sn bond in $EuSn_2P_2$.

DISCUSSION

In summary, we have conducted comprehensive studies of crystal structure, magnetic order, and valence state on the magnetic topological semimetal $EuSn_2P_2$ under pressure up to 62 GPa. XRD data reveals a rhombohedral-to-amorphous transition at 36 GPa and the amorphous phase remains up to 62 GPa. Pressure enhances the magnetic ordering temperature remarkably with an over four-fold increase from ambient pressure, attributed to the enhancement of RKKY interactions through stronger Eu-Sn bond under pressure. Eu ions remain mostly divalent until 20 GPa and enters an intermediate valence state at higher pressure up to 47 GPa. Band structure calculations in $EuSn_2P_2$ show that both change in lattice parameter and change in magnetic configuration from in-plane to out-of-plane will impact the topological properties, with the latter playing a dominant role. The experimentally observed in-plane spin orientation of Eu ions in the measured pressure range suggests that the any possible change of topological properties will be attributed to the change in lattice parameters. Our work establishes that pressure is an effective tuning parameter to elevate the magnetic ordering temperature, a critical parameter to realize novel quantum phases. These rich results pave the way for further experimental and theoretical efforts to explore the pressure-tuning of magnetism, possible superconductivity, and their interplay with crystal structure and topological electronic states.

METHODS

XRD

Single crystals of $EuSn_2P_2$ were grown by the Sn-flux method reported previously[15]. High-pressure XRD, SMS, and PFY- XAS experiments were carried out at the 13BM-C (PX^2), 3ID, and 16ID-D Beamlines, respectively, at the Advanced Photon Source, Argonne National Laboratory. Two runs of powder XRD experiments at high pressure and room temperature were conducted. X-rays with a wavelength of 0.434 Å were focused to 15 μm(v) × 15μm(h) size. A piece of single crystalline sample was ground into powder and loaded in the diamond anvil cell. In run 1 a BX90 diamond anvil cells (DAC) equipped with one pair of Boehler-Almax anvils of 500 μm diameter culet to allow large diffraction angles was used[36]. Helium was used as the pressure-transmitting medium up to 23.3 GPa. Ruby was used to determine pressure[37]. In run 2 a symmetric cell was used up to 62 GPa with cubic boron nitride seats and anvils of 300 μm diameter culet and neon pressure transmitting medium was used. Initial pressure was determined from ruby during Ne gas loading and subsequent pressures were determined in-situ from the equation of state of Au[38] at the same position where XRD data was taken on the sample. In both runs rhenium (Re) gaskets were used to contain the samples between the diamond anvils. The 2-D diffraction images were integrated using DIOPTAS software[39] and Rietveld refinements on the XRD data were performed in GSAS-II[40].

SMS under pressure

High-pressure ^{151}Eu SMS experiments were carried out to investigate the evolution of the magnetism of $EuSn_2P_2$. SMS, also known as nuclear forward scattering, utilizes the pulsed synchrotron X-ray to probe the nuclear spin transition in time domain. SMS is a sensitive probe

to study magnetic state down to the atomic level and is one of the few techniques compatible with extreme sample environments. The SMS experiments were performed during the standard 24-bunch timing mode of the APS with 153 ns separation between two successive electron bunches for data collection. The magnetism is probed through M1 transition 7/2 - 5/2 in ^{151}Eu at the nuclear resonant energy of 21.54 keV with high resolution monochromators[41]. X-rays were focused to 15 μm(v) × 15 μm(h) (FWHM). Low temperatures were achieved in a specially designed helium-flow cryostat[42]. High pressures were generated using a membrane-driven miniature panoramic DAC. Re gaskets were prepared and EDM-drilled to form the sample chamber.

Three experimental runs were performed with different sample loadings, run 1 up to 10.4 GPa, run 2 up to 22.7 GPa, and run 3 up to 41.2 GPa. A single crystalline sample was loaded in each run such that the incident X-ray is along the c-axis of the crystal. In run 1 and 2 helium was used as pressure medium to ensure hydrostatic pressure environment at low temperatures. In run 3 a neon pressure medium was used. After gas loading at room temperature, all subsequent pressures were applied through gas membrane at low temperature between 100 and 150 K. Pressures were determined from ruby scale[37]. At each pressure the SMS spectra were collected at various temperatures across the magnetic order. Possible valence transition of Eu ions in the sample can be detected by the change of the isomer shift. The isomer shift values were obtained in-situ by placing a reference sample with a known isomer shift value in the X-ray beam[33,43–45]. For divalent Eu ions in $EuSn_2P_2$, a trivalent reference sample Eu_2O_3 with an isomer shift of 1.024 mm/s (relative to EuF_3) was placed in the beam. SMS data together with the reference sample were collected in the paramagnetic phase of $EuSn_2P_2$ which simplifies the spectra due to the absence of magnetic hyperfine field.

High-pressure PFY-XAS

To provide direct information on Eu's valent state and confirm any possible changes suggested by the isomer shift measurements, XAS experiment was carried out at Eu's L L_3 edge (6.97 keV) up to 47 GPa. A single crystal sample was loaded in a symmetric-type DAC with beryllium gasket and an insert from cubic boron nitride and epoxy. Pressures were measured in-situ from ruby fluorescence. To avoid heavy absorption by diamond anvil at this energy, XAS was taken with the incident X-ray beam going through the Be gasket and absorption signal being taken in the fluorescence geometry using a Pilatus detector. The X-rays were focused to 5 μm (FWHM). The sample position at each pressure was carefully determined by scanning the sample position to minimize self-absorption. Ruby was used to determine the pressure in-situ[37].

Molecular orbital calculations

To provide insight to the enhanced T_o, we have performed molecular orbital calculations in $EuSn_2P_2$ at ambient and high pressure employing semi-empirical extended-Hückel-tight-binding (EHTB) methods and CAESAR packages[46]. The basis sets used in the the calculations of molecular orbitals of $EuSn_2P_2$ at ambient and high pressure for Eu are: 6s: Hii = -7.42 eV, ζ1 = 1.400, coefficient1 = 1.0000; 6p: Hii = -4.65 eV, ζ1 = 1.400, coefficient1 = 1.000; 5d: Hii = -8.08 eV, ζ1 = 2.753, coefficient1 = 0.7187, ζ1 = 1.267, coefficient2 = 0.4449; 4f: Hii = -11.28 eV, ζ1 = 6.907, coefficient1 = 0.7354, ζ1 = 2.639, coefficient2 = 0.4597. For Sn: 5s: Hii = -16.16 eV, ζ1 = 2.120, coefficient1 = 1.000; 5p: Hii = -8.32 eV, ζ1 = 1.820, coefficient1 = 1.000. For P: 3s: Hii = -18.60 eV, ζ1 = 1.750, coefficient1 = 1.000; 3p: Hii = -14.00 eV, ζ1 = 1.300, coefficient1 = 1.000.

DATA AVAILABILITY

The data that support the findings of this study are available from the corresponding author

upon reasonable request.

References

1. Hasan, M. Z. & Kane, C. L. Colloquium: Topological insulators. *Rev. Mod. Phys.* **82**, 3045–3067 (2010).
2. He, M., Sun, H. & He, Q. L. Topological insulator: Spintronics and quantum computations. *Front. Phys.* **14**, (2019).
3. Tokura, Y., Yasuda, K. & Tsukazaki, A. Magnetic topological insulators. *Nat. Rev. Phys.* **1**, 126–143 (2019).
4. Yu, R. *et al.* Quantized Anomalous Hall Effect in Magnetic Topological Insulators. *Science* **329**, 61–64 (2010).
5. Masuda, H. *et al.* Quantum Hall effect in a bulk antiferromagnet $EuMnBi_2$ with magnetically confined two-dimensional Dirac fermions. *Sci. Adv.* **2**, 1–7 (2016).
6. Deng, Y. *et al.* Quantum anomalous Hall effect in intrinsic magnetic topological insulator $MnBi_2Te_4$. *Science.* **367**, 895–900 (2020).
7. Mong, R. S. K., Essin, A. M. & Moore, J. E. Antiferromagnetic topological insulators. *Phys. Rev. B.* **81**, 245209 (2010).
8. Li, R., Wang, J., Qi, X.-L. & Zhang, S.-C. Dynamical axion field in topological magnetic insulators. *Nat. Phys.* **6**, 284–288 (2010).
9. Otrokov, M. M. *et al.* Prediction and observation of an antiferromagnetic topological insulator. *Nature* **576**, 416–422 (2019).
10. Zhang, D. *et al.* Topological Axion States in the Magnetic Insulator $MnBi_2Te_4$ with the Quantized Magnetoelectric. *Phys. Rev. Lett.* **122**, 206401 (2019).
11. Qi, X.-L., Hughes, T. L. & Zhang, S.-C. Chiral topological superconductor from the quantum Hall state. *Phys. Rev. B* **82**, 184516 (2010).
12. Hao, Y.-J. *et al.* Gapless Surface Dirac Cone in Antifer- romagnetic Topological Insulator $MnBi_2Te_4$, *Phys. Rev. X* **9**, 041038 (2019).
13. Li, J. *et al.* Intrinsic magnetic topological insulators in van der Waals layered $MnBi_2Te_4$ -family materials. *Sci. Adv.* **5**, eaaw5685 (2019).
14. Chen, B. *et al.* Intrinsic magnetic topological insulator phases in the Sb doped $MnBi_2Te_4$ bulks and thin flakes. *Nat. Commun.* **10**, 4469 (2019).
15. Gui, X. *et al.* A New Magnetic Topological Quantum Material Candidate by Design. *ACS Cent. Sci.* **5**, 900–910 (2019).
16. Wang, L. L. *et al.* Single pair of Weyl fermions in the half-metallic semimetal $EuCd_2As_2$. *Phys. Rev. B* **99**, 1–9 (2019).
17. Li, H. *et al.* Dirac Surface States in Intrinsic Magnetic Topological Insulators $EuSn_2As_2$ and $MnBi_{2n}Te_{3n+1}$. *Phys. Rev. X* **9**, 041039 (2019).
18. Xu, Y., Song, Z., Wang, Z., Weng, H. & Dai, X. Higher-Order Topology of the Axion Insulator $EuIn_2As_2$. *Phys. Rev. Lett.* **122**, 256402 (2019).
19. Zhang, H. *et al.* Topological insulators in Bi_2Se_3, Bi_2Te_3 and Sb_2Te_3 with a single Dirac cone on the surface. *Nat. Phys.* **5**, 438–442 (2009).
20. Ōnuki, Y. *et al.* Divalent, trivalent, and heavy fermion states in Eu compounds. *Philos. Mag.* **97**, 3399–3414 (2017).
21. Rosa, P. F. S. *et al.* Competing magnetic orders in the superconducting state of heavy-fermion $CeRhIn_5$. *Proc. Natl. Acad. Sci. U. S. A.* **114**, 5384–5388 (2017).

22. Wu, J. J. *et al.* Pressure-decoupled magnetic and structural transitions of the parent compound of iron-based 122 superconductors $BaFe_2As_2$. *Proc. Natl. Acad. Sci. U. S. A.* **110**, 17263–17266 (2013).
23. Zhao, L. *et al.* Monoclinic $EuSn_2As_2$: A Novel High-Pressure Network Structure -suppl. *Phys. Rev. Lett.* **126**, 155701 (2021).
24. Birch, F. Finite strain isotherm and velocities for single-crystal and polycrystalline NaCl at high pressures and 300°K. *J. Geophys. Res.* **83**, 1257 (1978).
25. Bauer, R., Tse, J. S., Komatsu, K., Machida, S. & Hattori, T. Slow compression of crystalline ice at low temperature. *Nature* **585**, E9–E10 (2020).
26. Sankaran, H., Sharma, S. M., Sikka, S. K. & Chidambaram, R. Pressure induced amorphization of $AlPO_4$. *Pramana* **35**, 177–180 (1990).
27. Tse, J. S. & Klug, D. D. Structural Memory in Pressure-Amorphized $AlPO_4$. *Science* **255**, 1559–1561 (1992).
28. Liu, H. *et al.* Mechanisms for pressure-induced crystal-crystal transition, amorphization, and devitrification of SnI_4. *J. Chem. Phys.* **143**, 164508 (2015).
29. Wang, Y. *et al.* Reversible switching between pressure-induced amorphization and thermal-driven recrystallization in VO_2(B) nanosheets. *Nat. Commun.* **7**, 1–8 (2016).
30. Yu, F. H. *et al.* Elevating the magnetic exchange coupling in the compressed antiferromagnetic axion insulator candidate $EuIn_2As_2$, *Phys. Rev. B* **102**, 180404 (2020).
31. Deb, S. K., Wilding, M., Somayazulu, M. & McMillan, P. F. Pressure-induced amorphization and an amorphous - Amorphous transition in densified porous silicon. *Nature* **414**, 528–530 (2001).
32. Sturhahn, W. CONUSS and PHOENIX: Evaluation of nuclear resonant scattering data. *Hyperfine Interact.* **125**, 149–172 (2000).
33. Bi, W. *et al.* Synchrotron x-ray spectroscopy studies of valence and magnetic state in europium metal to extreme pressures. *Phys. Rev. B* **85**, 205134 (2012).
34. Coey, J. M. D. Amorphous magnetic order. *J. Appl. Phys.* **49**, 1646–1652 (1978).
35. Pierantozzi, G. M. *et al.* Evidence of magnetism-induced topological protection in the axion insulator candidate EuSn 2 P 2. *Proc. Natl. Acad. Sci.* **119**, e2116575119 (2022).
36. Kantor, I. *et al.* BX90: A new diamond anvil cell design for X-ray diffraction and optical measurements. *Rev. Sci. Instrum.* **83**, (2012).
37. Dewaele, A., Torrent, M., Loubeyre, P. & Mezouar, M. Compression curves of transition metals in the Mbar range: Experiments and projector augmented-wave calculations. *Phys. Rev. B - Condens. Matter Mater. Phys.* **78**, 1–13 (2008).
38. Fei, Y. *et al.* Toward an internally consistent pressure scale. *Proc. Natl. Acad. Sci.* **104**, 9182–9186 (2007).
39. Prescher, C. & Prakapenka, V. B. DIOPTAS : a program for reduction of two-dimensional X-ray diffraction data and data exploration. *High Press. Res.* **35**, 223–230 (2015).
40. Toby, B. H. & Von Dreele, R. B. GSAS-II : the genesis of a modern open-source all purpose crystallography software package. *J. Appl. Crystallogr.* **46**, 544–549 (2013).
41. Leupold, O. *et al.* Nuclear resonance scattering of synchrotron radiation at the 21.5 keV resonance of 151 Eu. *Europhys. Lett.* **35**, 671–676 (1996).
42. Zhao, J. Y. *et al.* A compact membrane-driven diamond anvil cell and cryostat system for nuclear resonant scattering at high pressure and low temperature. *Rev. Sci. Instrum.* **88**, 125109 (2017).
43. Wortmann, G., Ponkratz, U., Bielemeier, B. & Rupprecht, K. Phonon density-of-states in

bcc and hcp Eu metal under high pressure measured by 151 Eu nuclear inelastic scattering of synchrotron radiation. *High Press. Res.* **28**, 545–551 (2008).
44. Souza-Neto, N. M. *et al.* Reentrant valence transition in EuO at high pressures: Beyond the bond-valence model. *Phys. Rev. Lett.* **109**, 026403–4 (2012).
45. Bi, W. *et al.* Microscopic phase diagram of $Eu(Fe_{1-x}Ni_x)As_2$ (x = 0,0.04) under pressure. *Phys. Rev. B* **103**, 195135 (2021).
46. Hoffmann, R. An Extended Hückel Theory. I. Hydrocarbons. *J. Chem. Phys.* **39**, 1397–1412 (1963).

ACKNOWLEDGMENTS

We thank G. Fabbris for critical reading of the manuscript and helpful discussion. This work is supported by the National Science Foundation (NSF) through Grant No. OIA-2033131. T. Culverhouse acknowledges the support provided by the National Aeronautics and Space Administration (NASA)-Alabama Space Grant Consortium, Research Experiences for Undergraduates (REU) award to University of Alabama at Birmingham. Z. Nix acknowledges the support from the Department of Education-Graduate Assistantship in Areas of National Need (GAANN) Grant No. P200A180001. W. Xie is supported by Department of Energy under the contract of DE-SC0022156. This research used resources of the Advanced Photon Source (APS), Argonne National Laboratory (ANL), a U.S. Department of Energy (DOE) Office of Science User Facility operated for the DOE Office of Science by Argonne National Laboratory under Contract No. DE- AC02-06CH11357. Portions of this work were performed at HPCAT (Sector 16), APS, ANL. HPCAT operations are supported by DOE-NNSA's Office of Experimental Sciences. Support from COMPRES under NSF Cooperative Agreement EAR-1606856 is acknowledged for COMPRES-GSECARS gas loading system and the PX^2 program. We are grateful to S. Tkachev for help with the gas loading of the DACs at the APS.

AUTHOR CONTRIBUTIONS

W.B. designed this research project. W.B., T.C., Z.N., J.Z., B.L., E.E.A, D.Z, J.X., Y.X., and Y.K.V. performed the experiments. W.X. synthesize the $EuSn_2P_2$ sample and performed the molecular orbital calculations. T.C conducted the GGA calculations. W.B., T.C., and U.D. analyzed the data. W.B. and W.X. wrote the manuscript with input from all authors.

COMPETING INTERESTS

The authors declare no competing interests.

ADDITIONAL INFORMATION

Correspondence and requests for materials should be addressed to Wenli Bi.

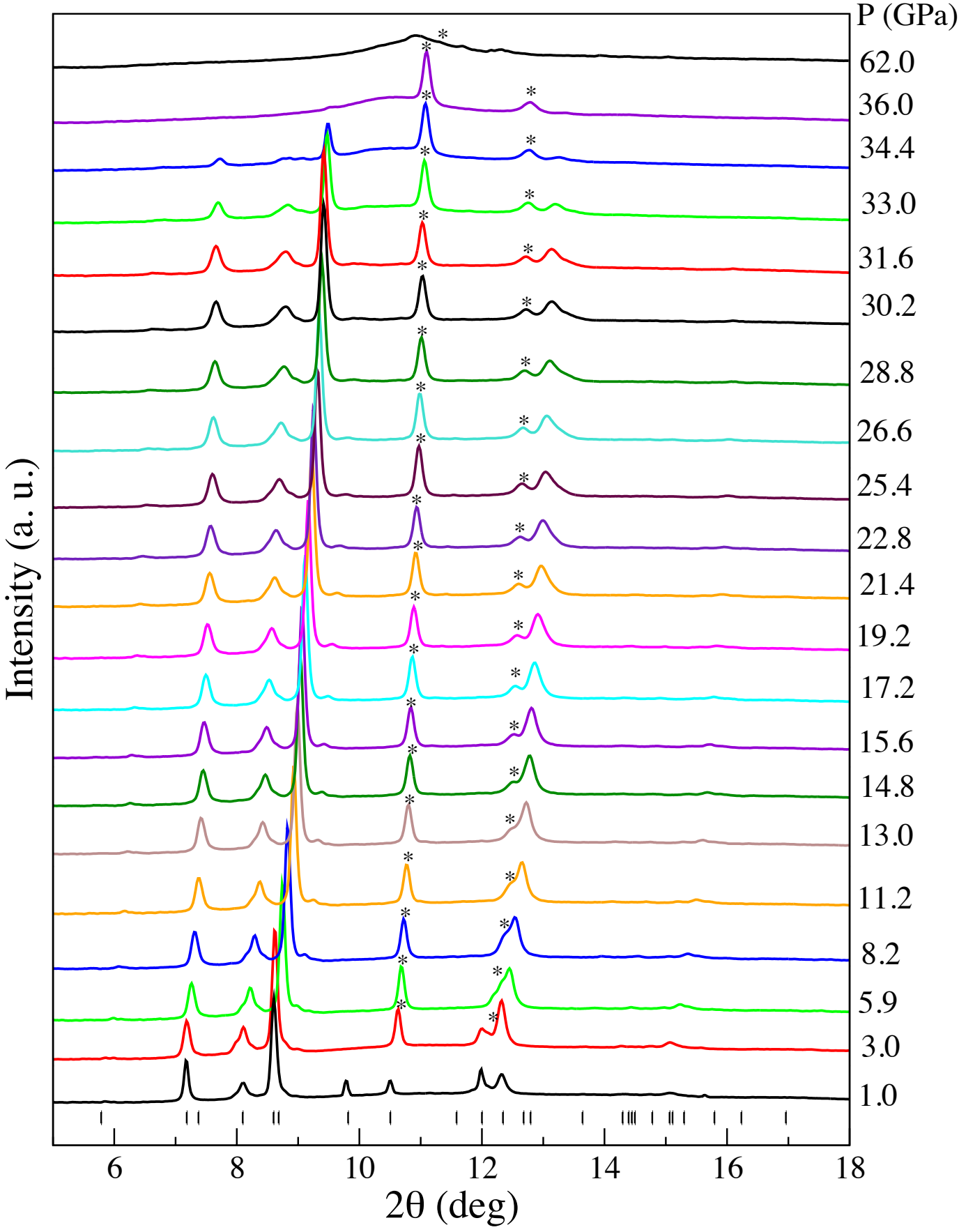
P (GPa)
62.0
36.0
34.4
33.0
31.6
30.2
28.8
26.6
25.4
22.8
21.4
19.2
17.2
15.6
14.8
13.0
11.2
8.2
5.9
3.0
1.0
Intensity (a. u.)
6
8
10
12
14
16
18
2θ (deg)

Table 1. Isomer shift (δ) values of ^{151}Eu in $EuSn_2P_2$ relative to Eu_2O_3 at various pressures and temperatures.

P(GPa)	T (K)	δ (mm/s)
1.0	300	-10.30 (1)
1.9	110	-10.25 (2)
3.0	300	-9.99 (1)
3.7	100	-9.98 (1)
7.3	100	-9.48 (1)
10.4	100	-9.15 (3)
16.0	105	-8.25 (1)
20.7	110	-6.67 (4)
28.9	130	-6.26 (1)
41.2	160	-5.39 (6)

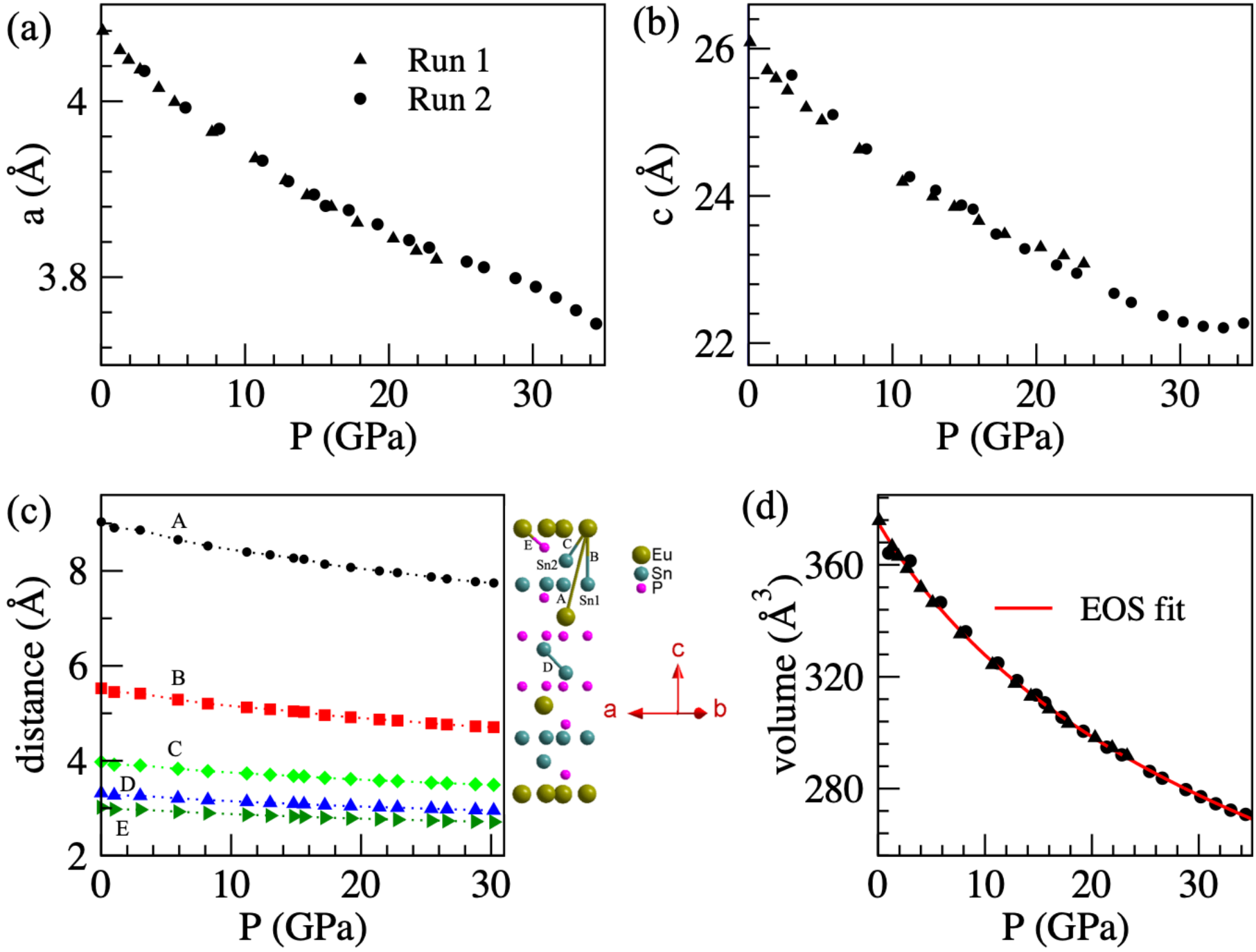
(a)
Run 1
Run 2
a (Å)
4
3.8
0
10
20
30
P (GPa)
(b)
c (Å)
26
24
22
0
10
20
30
P (GPa)
(c)
distance (Å)
8
6
4
2
A
B
C
D
E
0
10
20
30
P (GPa)
E
C
B
Sn2
A
Sn1
D
Eu
Sn
P
c
a
b
(d)
volume (Å^3)
360
320
280
EOS fit
0
10
20
30
P (GPa)

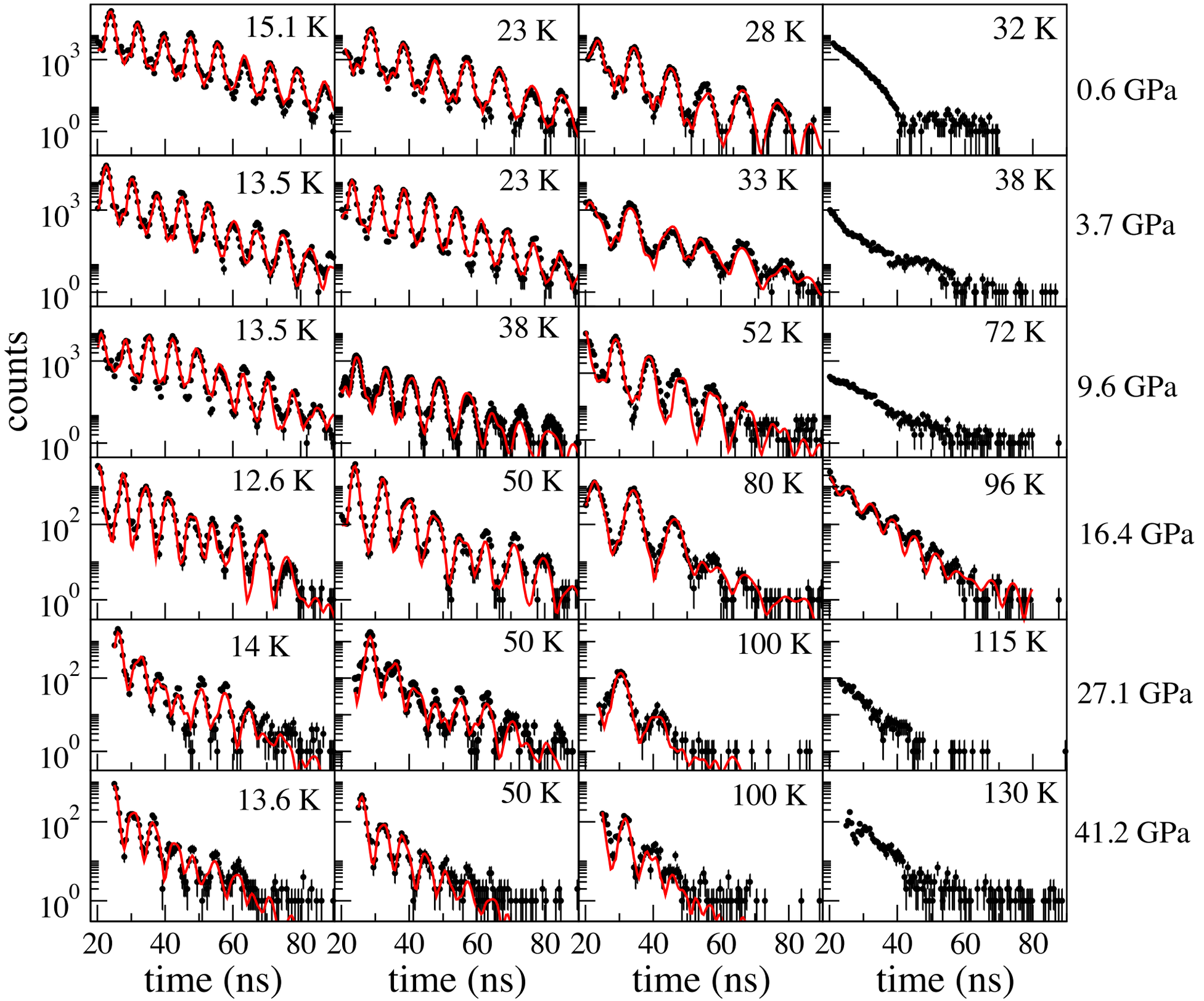
15.1 K
23 K
28 K
32 K
0.6 GPa
13.5 K
23 K
33 K
38 K
3.7 GPa
13.5 K
38 K
52 K
72 K
9.6 GPa
12.6 K
50 K
80 K
96 K
16.4 GPa
14 K
50 K
100 K
115 K
27.1 GPa
13.6 K
50 K
100 K
130 K
41.2 GPa
counts
time (ns)
time (ns)
time (ns)
time (ns)

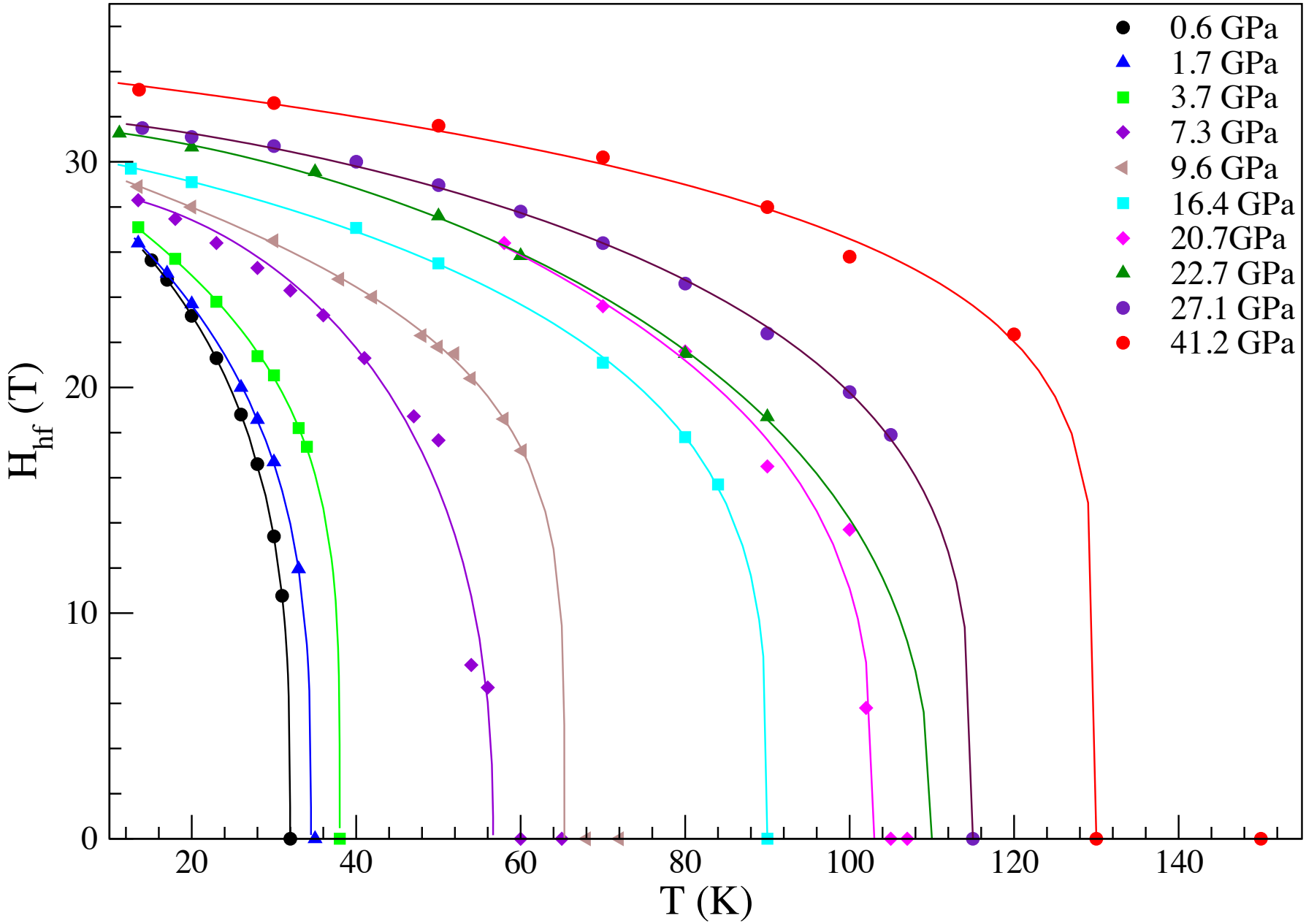
0.6 GPa
1.7 GPa
3.7 GPa
7.3 GPa
9.6 GPa
16.4 GPa
20.7GPa
22.7 GPa
27.1 GPa
41.2 GPa
H_hf (T)
T (K)
0
10
20
30
20
40
60
80
100
120
140

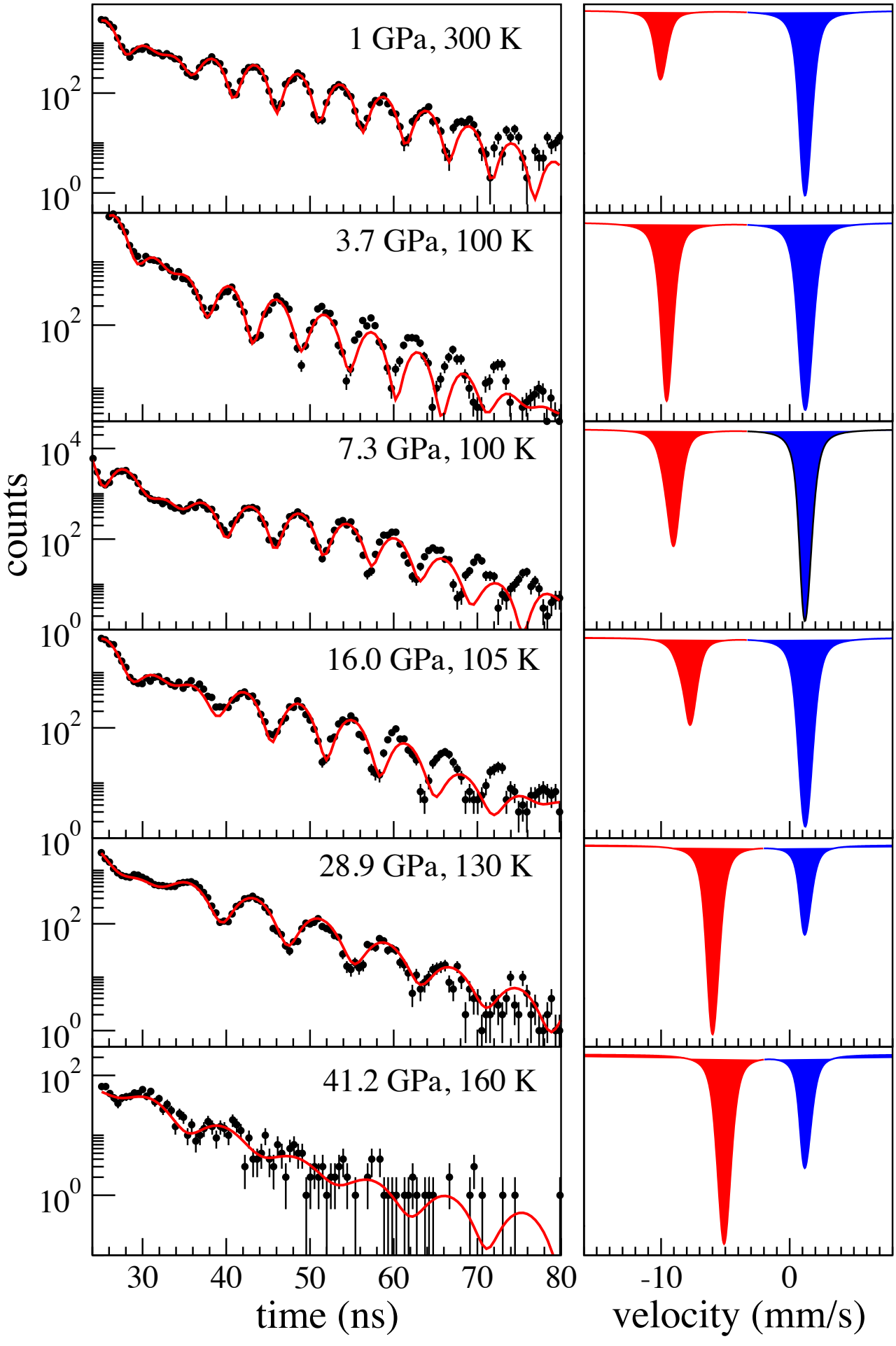
1 GPa, 300 K
3.7 GPa, 100 K
7.3 GPa, 100 K
16.0 GPa, 105 K
28.9 GPa, 130 K
41.2 GPa, 160 K
counts
time (ns)
velocity (mm/s)

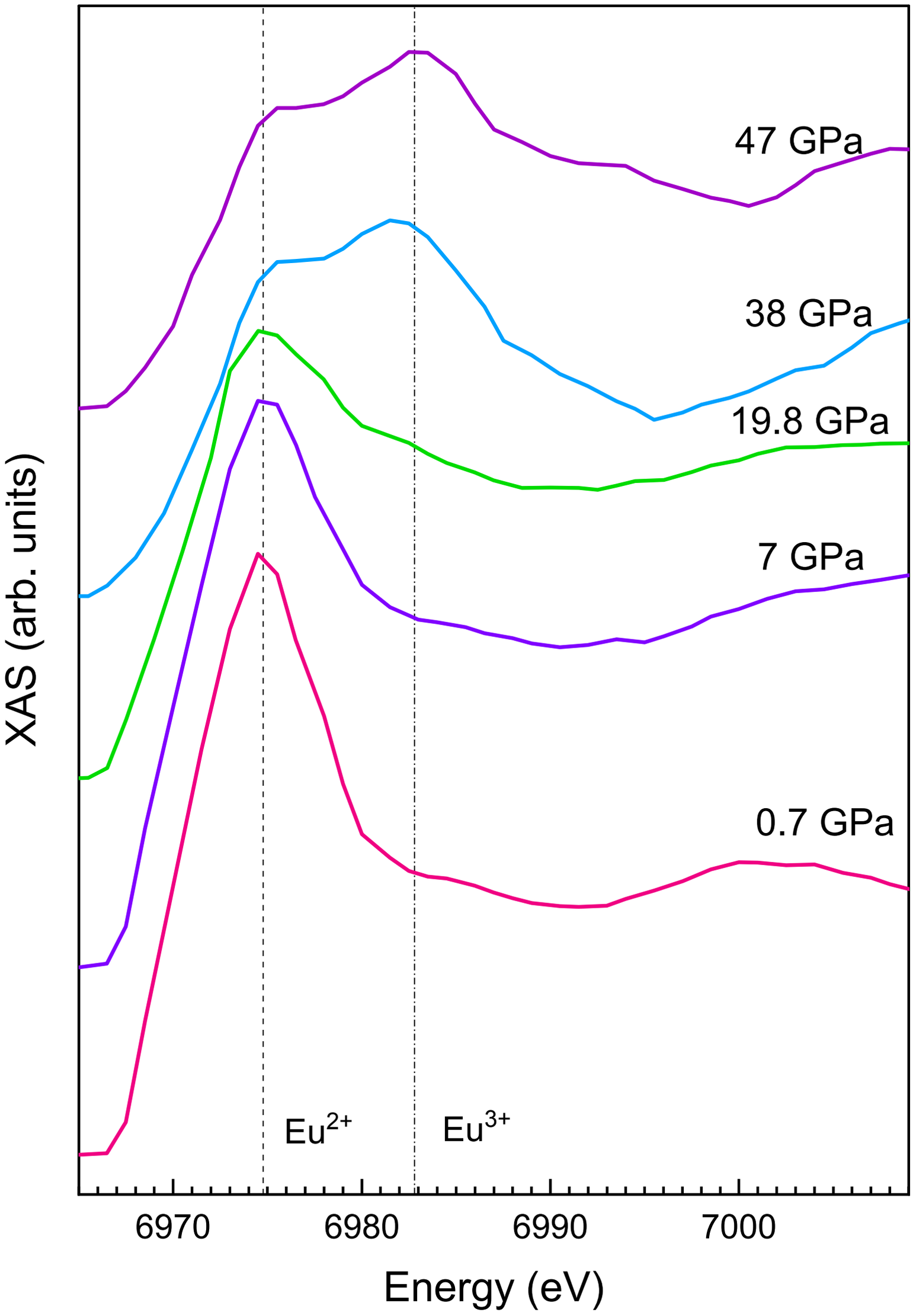
47 GPa
38 GPa
19.8 GPa
7 GPa
0.7 GPa
Eu2+
Eu3+
XAS (arb. units)
6970
6980
6990
7000
Energy (eV)

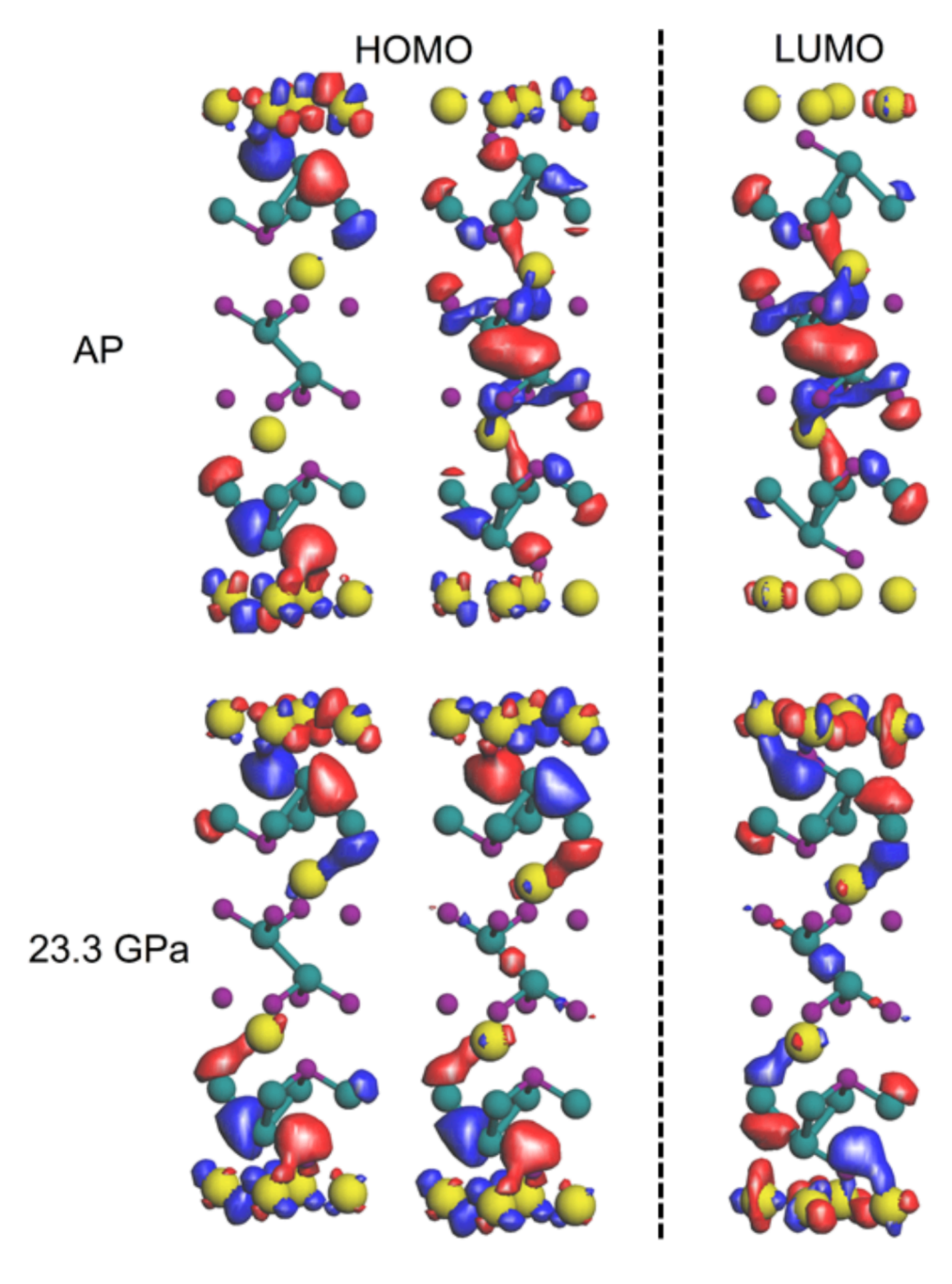
HOMO
LUMO
AP
23.3 GPa

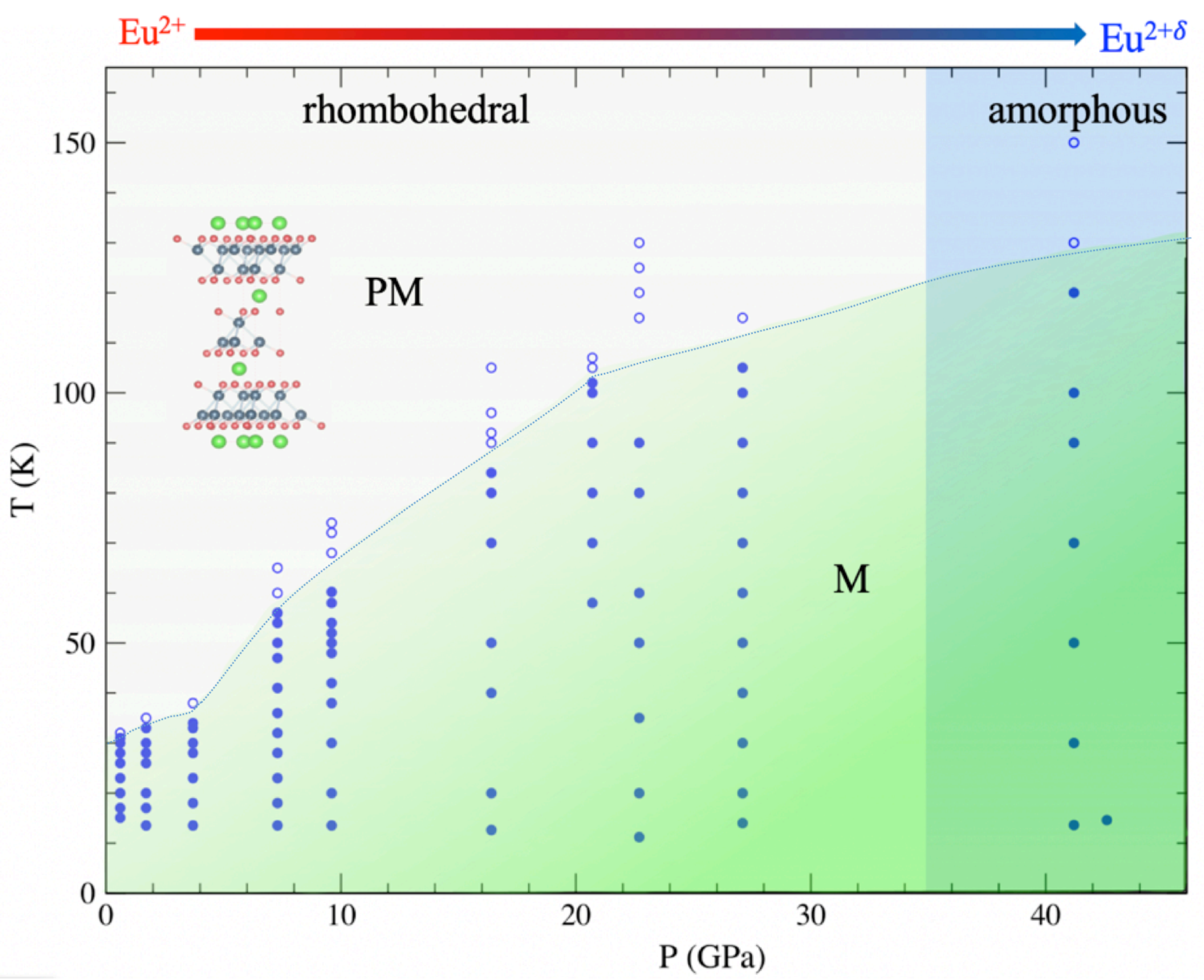
Eu2+
Eu2+δ
rhombohedral
amorphous
PM
M
150
100
50
0
T (K)
0
10
20
30
40
P (GPa)